



ELSEVIER

Available online at [www.sciencedirect.com](http://www.sciencedirect.com)

ScienceDirect

journal homepage: [www.elsevier.com/locate/he](http://www.elsevier.com/locate/he)

# Facile preparation of BiVO<sub>4</sub>/FeVO<sub>4</sub> heterostructure for efficient water-splitting applications

Ning Li <sup>a</sup>, Xiaofeng Wu <sup>a</sup>, Meng Wang <sup>a</sup>, Keke Huang <sup>a</sup>, Jingjing He <sup>a</sup>, Wei Ma <sup>a</sup>, Huanwen Chen <sup>a</sup>, Yue Li <sup>b</sup>, Shouhua Feng <sup>a,\*</sup>

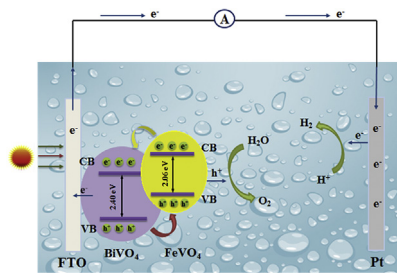
<sup>a</sup> State Key Laboratory of Inorganic Synthesis and Preparative Chemistry, College of Chemistry, Jilin University, Changchun, 130012, PR China

<sup>b</sup> Changchun Institute of Optics, Fine Mechanics and Physics, Chinese Academy of Sciences, No.3888, Dong Nanhu Road, Changchun, Jilin Province, 130033, China

## HIGHLIGHTS

- A BiVO<sub>4</sub>/FeVO<sub>4</sub> heterostructure was successfully synthesized by electrospray technique.
- Charge transfer kinetics of BiVO<sub>4</sub> was greatly promoted after modification by FeVO<sub>4</sub>.
- This work offers a facile strategy to prepare nanocomposites for PEC water oxidation.

## GRAPHICAL ABSTRACT



## ARTICLE INFO

### Article history:

Received 27 March 2019

Received in revised form

25 June 2019

Accepted 6 July 2019

Available online 7 August 2019

### Keywords:

BiVO<sub>4</sub>/FeVO<sub>4</sub> heterostructure

Electrospray technique

Photoelectrochemical water oxidation

## ABSTRACT

In this paper, a BiVO<sub>4</sub>/FeVO<sub>4</sub> heterostructure photoanode was synthesized by electrospray technique, and its photoelectrochemical water oxidation performance was investigated. The maximum photocurrent density of  $0.4 \text{ mA cm}^{-2}$  at  $1.23 \text{ V}_{\text{RHE}}$  was 6 times higher than that of pristine BiVO<sub>4</sub> films ( $0.06 \text{ mA cm}^{-2}$ ). Through the analysis of the electrochemical impedance spectroscopy (EIS) results, the improvement of photoelectrochemical performance could be attributed to the formation of heterostructure at the two-phase interface, which led to the effective separation of electron-hole pairs. This work offers a new effective strategy to construct semiconductor nanocomposites for efficient photoelectrochemical water oxidation.

© 2019 Hydrogen Energy Publications LLC. Published by Elsevier Ltd. All rights reserved.

\* Corresponding author.

E-mail address: [shfeng@mail.jlu.edu.cn](mailto:shfeng@mail.jlu.edu.cn) (S. Feng).

<https://doi.org/10.1016/j.ijhydene.2019.07.063>

0360-3199/© 2019 Hydrogen Energy Publications LLC. Published by Elsevier Ltd. All rights reserved.

## Introduction

Photoelectrochemical (PEC) cell is the most advanced way to store hydrogen energy by converting solar energy into chemical energy [1–4]. Since the application of TiO<sub>2</sub> electrodes for water-splitting, many semiconductors such as WO<sub>3</sub>, Fe<sub>2</sub>O<sub>3</sub> and ZnO have been found to show photoelectrochemical activity. However, most of them have the disadvantages of improper band gap and rapid recombination of photo-generated charge carriers, which are considered to be important factors to cause low solar-to-hydrogen conversion efficiency [5–8]. Recently, BiVO<sub>4</sub> ( $E_g = 2.40$  eV) has become excellent candidate for water-splitting applications due to its appropriate electronic band gap, excellent chemical and thermal stabilities, and environmental friendliness. However, the poor separation ability and the slow mobility of carriers have limited photocatalytic efficiency in practical applications [9–11].

In order to overcome the problem of rapid recombination of carriers, a lot of efforts have been made, such as controlling morphology [12], doping [13,14], and coupling with oxygen-evolution cocatalysts (OECs) [15]. In addition, one of the appealing strategies is fabricating heterostructure by coupling narrow optical band gap semiconductors, such as Cu<sub>2</sub>O, CuWO<sub>4</sub>, FeVO<sub>4</sub> with BiVO<sub>4</sub> [16–18]. Among them, FeVO<sub>4</sub> is considered to be the most promising candidate because of its wide visible light absorption and suitable band gap [19,20]. Theoretically, FeVO<sub>4</sub> and BiVO<sub>4</sub> have good band matching. When two semiconductors are coupled, photogenerated electrons can be injected into the BiVO<sub>4</sub> from the conduction band of FeVO<sub>4</sub>, which provides a new idea to solve the weakness of fast carrier recombination rate of BiVO<sub>4</sub> materials. Recently, Muhammad and his co-works were reported to have successfully synthesized BiVO<sub>4</sub>/FeVO<sub>4</sub> nanocomposite electrodes by hydrothermal method, and their photocatalytic activity was investigated by decomposing crystal violet (CV) organic dyes. The results showed that the 2:1 ratio of BiVO<sub>4</sub>/FeVO<sub>4</sub> could completely degrade CV within 60 min [21]. Moreover, Maheswari used template-assisted method to synthesize a BiVO<sub>4</sub>/FeVO<sub>4</sub> heterostructure photoanode. The photoelectrode exhibited a photocurrent density of 2.5 mA cm<sup>-2</sup> at 1.23 V<sub>RHE</sub>, which might be attributed to excellent charge transfer/transport phenomena [18].

Semiconductor materials were widely synthesized in several ways such as sol-gel method [22], hydro-thermal method [23], PLD [24], CVD [25]. As recent examples, Sang and his co-works synthesized TiO<sub>2</sub> nanoparticle films at room temperature by PLD technology. The results showed that when the film thickness was less than 400 nm, the highest photocurrent density (0.2 mA cm<sup>-2</sup>) and the best carrier separation efficiency were displayed [26]. Jennifer prepared a Fe<sub>2</sub>O<sub>3</sub>/Fe<sub>3</sub>O<sub>4</sub> composite film by one-step chemical vapor deposition and used it as an efficient photoanode material for PEC setups. The maximum photocurrent density of 0.48 mA cm<sup>-2</sup> at 1.23 V<sub>RHE</sub> was found under 1 sun illumination [27]. These traditional methods have their unique advantages, but they also have some shortcomings, such as complex

preparation process and serious waste of raw materials. Recently, the electrospray (ES) technique has aroused big interest, due to its ability to deposit high-quality films through the production of fine, highly wettable nano-droplets [28]. These highly charged droplets can be accelerated towards a substrate in the process of electrospray, and a well targeting property can result in low material consumption and high deposition efficiency [29]. Moreover, electrospray technique is simple, non-toxic, green and excellent control of stoichiometry. The nanoparticles prepared by this method are uniform in size, and the crystallinity and morphology of the films can be well controlled by adjusting the conditions such as voltage, substrate temperature, flow rate, and precursor concentration [30].

In this paper, The BiVO<sub>4</sub>/FeVO<sub>4</sub> heterojunction films were fabricated via electrospray technique for photoelectrochemical water splitting. As a result, the photocurrent density of the BiVO<sub>4</sub>/FeVO<sub>4</sub> heterojunction films was 6 times higher than that of pristine BiVO<sub>4</sub> films under 1 sun illumination. In addition, the IPCE increased from 2.5% to 13% at 450 nm. The enhanced performance might be attributed to the excellent charge transfer and separation phenomena, which was confirmed by EIS results.

## Experimental section

### Synthesis of BiVO<sub>4</sub>, FeVO<sub>4</sub>, and BiVO<sub>4</sub>/FeVO<sub>4</sub> heterojunction films

All the samples were synthesized by using a self-made equipment (Fig. S1). The precursor was pumped through the nozzle to produce charged micro-droplets, these micro-droplets were extremely small in size and had a well targeting property under the effects of a high voltage power. N<sub>2</sub> was used as a carrier gas to assist in atomizing droplets. A pre-cleaned FTO was used as the substrate and its temperature could be controlled by the connected heater.

The precursor solutions of BiVO<sub>4</sub> and FeVO<sub>4</sub> films were prepared by dissolving 0.1940 g bismuth nitrate pentahydrate, 0.1616 g iron (III) nitrate nonahydrate and 0.0467 g ammonium metavanadate in 20 mL ethylene glycol, respectively. BiVO<sub>4</sub> and FeVO<sub>4</sub> films were prepared by depositing 400 μL precursor solutions at 350 °C on the substrate. Subsequently, the BiVO<sub>4</sub>/FeVO<sub>4</sub> heterojunction films with different film thickness ratios (3:1, 2:1, 1:1, 1:2, 1:3) were prepared by controlling the ratio of the amount of precursor solutions of FeVO<sub>4</sub> and BiVO<sub>4</sub> (The total amount of precursor solutions is 400 μL). After each deposition, the samples were annealed at 500 °C for 2.5 h to ensure the crystallinity of the films.

### Characterization

The crystal structure of the samples was identified by X-ray diffraction (XRD) using a Rigaku D/Max 2500 V/PC instrument operating at 50 kV and 200 mA. The microstructures of the samples were observed using scanning electron microscopy (SEM, Helios Nano-lab 600i from FEI Company) and

transmission electron microscopy (TEM, FEI Tecnai G2 S-Twin F20). The surface chemical state and composition of the samples were examined by X-ray photoelectron spectroscopy (XPS, Thermo ESCALAB 250 spectrometer). Raman spectra measurements were recorded on a miniature (BWTek) Raman spectrometer (BTR-111) using 532 nm irradiation. The UV-vis diffuse reflectance spectra were measured on a Shimadzu UV-3600 UV/vis/NIR spectrophotometer.

Photoelectrochemical experiments were performed in a three-electrode system (CHI-660E, CH instruments Inc., Shanghai). The illumination area of the electrode was  $0.502 \text{ cm}^2$ , and 0.2 M aqueous solution of  $\text{Na}_2\text{SO}_4$  ( $\text{pH} = 7$ ) was utilized as the electrolyte. A 500 W xenon lamp was used as the light source, and the intensity was controlled at  $100 \text{ mW cm}^{-2}$ . In the experiment, The  $\text{BiVO}_4/\text{FeVO}_4$  heterojunction films (1:1) were proved to have the best photoelectrochemical properties, and the characterization of composite electrodes was based on this in the paper.

## Results and discussion

The crystalline structures of samples were characterized by XRD, and the results were shown in Fig. 1a. The high intensity

peaks at 26.5, 37.8, and 51.6 of all samples were due to FTO substrate. In the XRD pattern of a bare  $\text{BiVO}_4$  film, all diffraction peaks corresponded to monoclinic  $\text{BiVO}_4$  (JCPDS 83-1700). Compared to other crystal phases, only monoclinic phase  $\text{BiVO}_4$  had good photocatalytic activity [31]. Similarly, In the XRD pattern of a bare  $\text{FeVO}_4$  film, the peaks at 16.6, 17.5, 25.2, 27.1, 27.8, 31.3 and 42.1 corresponded to the (011), (-111), (012), (-201), (-211), (-122) and (-310) of triclinic  $\text{FeVO}_4$  (JCPDS 71-1592), respectively. As for the XRD pattern of the  $\text{BiVO}_4/\text{FeVO}_4$  heterojunction film, the main diffraction peaks were derived from monoclinic  $\text{BiVO}_4$  and triclinic  $\text{FeVO}_4$  nanocrystals. This indicated that  $\text{BiVO}_4$  and  $\text{FeVO}_4$  coexist in the composites, which provided an opportunity to form a heterojunction at the interface of the two phases. The conclusion was further confirmed in the Raman spectroscopy (Fig. S2).

Fig. 1b-d depicted scanning electron microscopy (SEM) images of all samples.  $\text{BiVO}_4$  showed a particulate, porous and worm-like morphology with the sizes of 200–300 nm and thickness of 390 nm (Fig. 1b). Well-developed porosity was advantageous for high photoactivity because of the smaller transmission distance of photogenerated carriers [32]. Fig. 1c displayed the  $\text{FeVO}_4$  films prepared by the same method,  $\text{FeVO}_4$  showed smaller grain sizes than  $\text{BiVO}_4$  (100–200 nm), and the thickness of the films was approximately 400 nm.

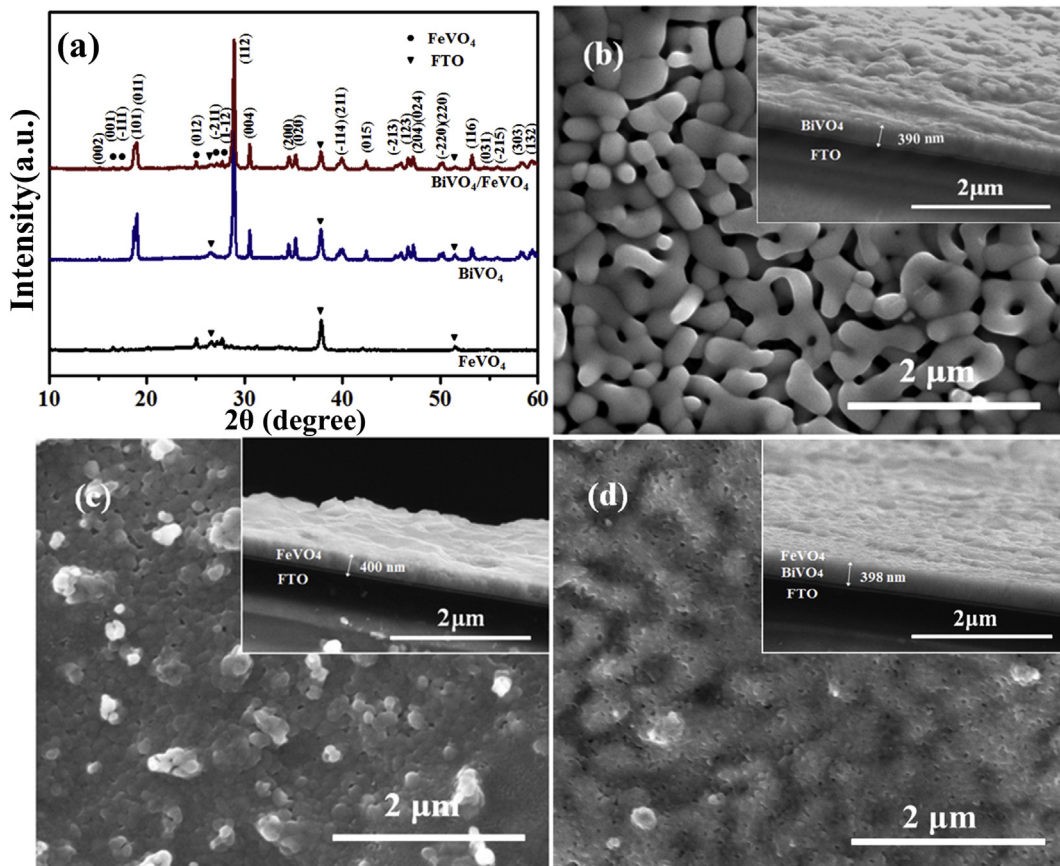


**Fig. 1 – (a)** XRD patterns of  $\text{BiVO}_4/\text{FTO}$ ,  $\text{FeVO}_4/\text{FTO}$ , and  $\text{BiVO}_4/\text{FeVO}_4/\text{FTO}$  heterojunction films. **SEM images of (b)**  $\text{BiVO}_4$ , **(c)**  $\text{FeVO}_4$ , **(d)**  $\text{BiVO}_4/\text{FeVO}_4$  heterojunction films.

**Fig. 1d** showed the surface and cross-sectional images of BiVO<sub>4</sub>/FeVO<sub>4</sub> heterojunction films. It could be seen that FeVO<sub>4</sub> nanoparticles were uniformly deposited on the BiVO<sub>4</sub> films and the thickness of the films was approximately 398 nm. The composition of the samples was further characterized by EDS (**Fig. S3**), the results showed that the BiVO<sub>4</sub>/FeVO<sub>4</sub> heterojunction films were composed of Bi, Fe, V and O elements, the appearance of the Si and Sn element peaks were due to the FTO substrate, and the element/atom composition conformed to the original feed ratio. In addition, FESEM-EDS mappings indicated intuitively that Bi, Fe, O and V elements were evenly spread in the composites (**Fig. S4**).

The chemical states of the samples were characterized by X-ray photoelectron spectroscopy (XPS). The survey scan (**Fig. 2a**) displayed that BiVO<sub>4</sub>/FeVO<sub>4</sub> heterojunction films contained Bi, Fe, O, V, C elements. Subsequently, the high-resolution XPS spectra of Bi 4f and Fe 2p were analyzed in two single-phase and the composites, the results were shown in **Fig. 2b** and **2c**, respectively. The Bi 4f peaks were observed at 158.6 eV and 163.9 eV, indicating that the valence of Bi is +3 [33]. The Fe 2p<sub>3/2</sub> spectra appeared at 710.79 eV, indicating that the valence of Fe is +3 [34]. Interestingly, compared with BiVO<sub>4</sub> and FeVO<sub>4</sub>, the binding energy of Bi 4f and Fe 2p for the BiVO<sub>4</sub>/FeVO<sub>4</sub> heterojunction films shifted to the higher binding energy, the transformation could be attributed to the

entanglement of FeVO<sub>4</sub> and BiVO<sub>4</sub> nanocrystals at the two-phase interface and the diffusion of carriers in the two semiconductors. The O 1s peaks of all samples were analyzed in **Fig. 2d**. The spectrum of O 1s was located at about 529.6 eV and 531.9 eV attributed to two different kinds of O species, respectively [35]. The binding energy of the O 1s peak in the BiVO<sub>4</sub>/FeVO<sub>4</sub> heterojunction film was shifted at 529.6 eV, which was due to the effect of oxygen vacancies and surface absorption of oxygen.

The microstructures of the BiVO<sub>4</sub>/FeVO<sub>4</sub> heterojunction films were performed by the transmission electron microscopy (TEM) and the high-resolution transmission electron microscopy (HRTEM). The low-magnification TEM image was showed in **Fig. 3a**, indicating that the BiVO<sub>4</sub>/FeVO<sub>4</sub> heterojunction films were composed of interconnected nanoparticles. Meanwhile, the high-resolution image showed the simultaneous presence of FeVO<sub>4</sub> and BiVO<sub>4</sub> lattices in the composites (**Fig. 3b**), suggesting that the heterostructure might be formed at the two-phase interface. The measured lattice spacing of 0.3731 nm could be indexed to the (−233) reflections of monoclinic BiVO<sub>4</sub> nanoparticles, the measured lattice spacing of 0.2047 nm could be indexed to the (1–13) reflections of triclinic structured FeVO<sub>4</sub> nanoparticles.

The optical properties of the samples were investigated by UV–Vis absorbance spectra, and the results were shown in

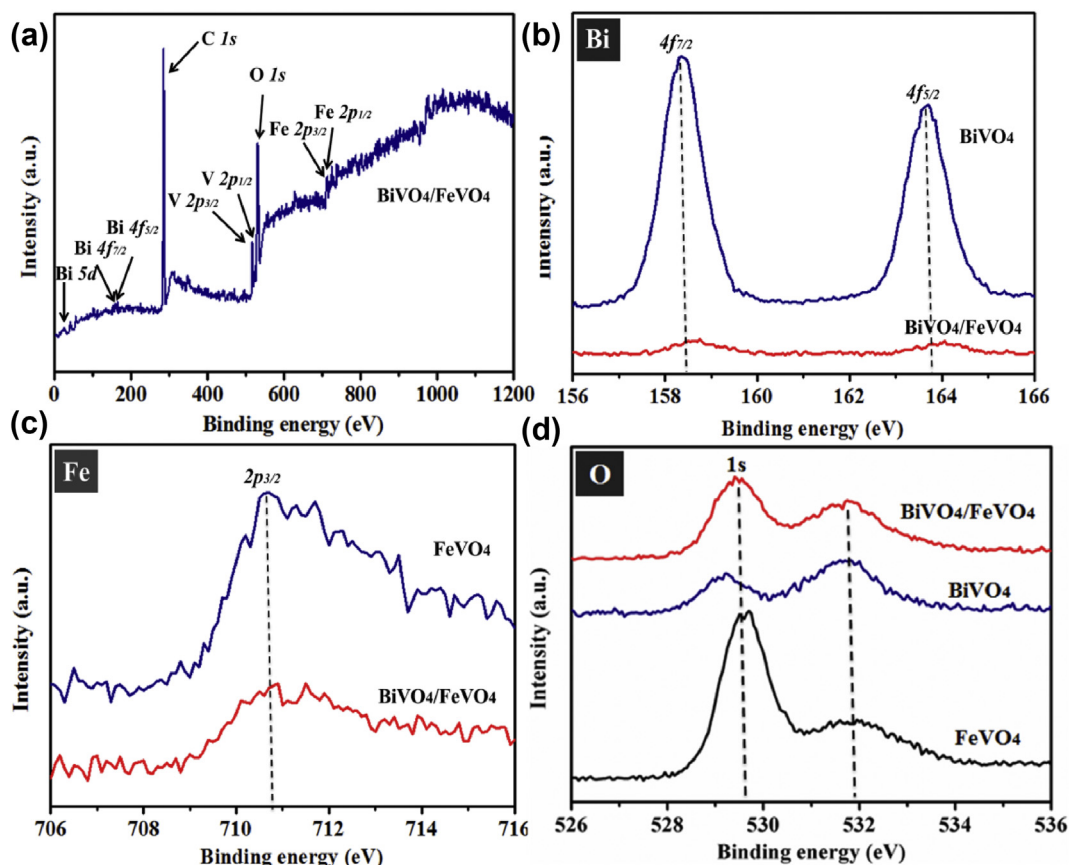


**Fig. 2 – XPS spectra of (a) the survey, (b) Bi 4f, (c) Fe 2p, and (d) O 1s.**

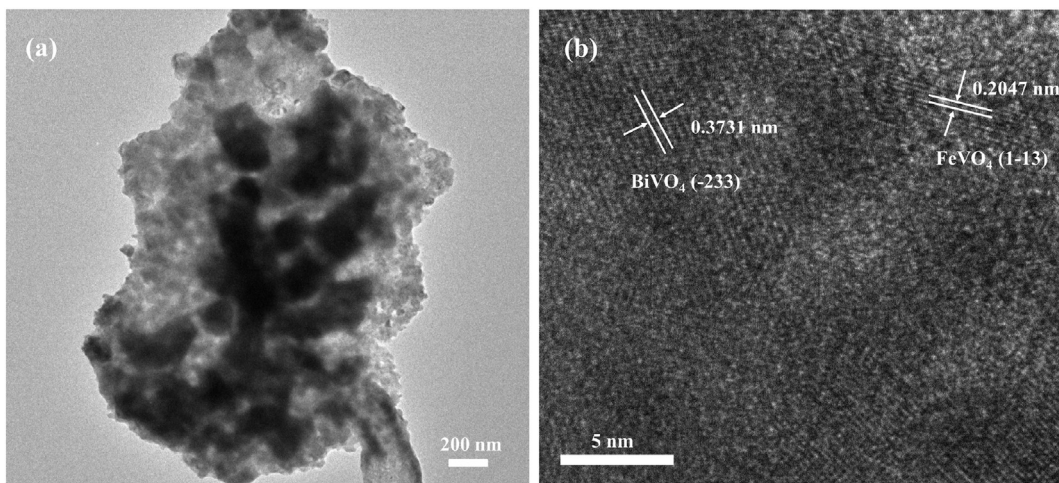


**Fig. 3 – TEM images of (a) and HRTEM images of the  $\text{BiVO}_4/\text{FeVO}_4$  heterojunction films (b).**

**Fig. 4.** The light absorption of bare  $\text{BiVO}_4$  started at around 520 nm. For  $\text{FeVO}_4$  films, the onset of light absorption was around 600 nm. The  $\text{BiVO}_4/\text{FeVO}_4$  heterojunction films exhibited a red shift toward a longer wavelength than  $\text{BiVO}_4$ , which indicated that the composite electrodes had excellent band alignment and broad visible light absorption due to the modification of  $\text{FeVO}_4$  layers.

Based on  $\text{BiVO}_4$ , the optimum temperature for samples deposition was determined (**Fig. S5a**). The results showed that the samples prepared at a substrate temperature of 350 °C had the largest photocurrent density. The phenomenon reflected the compromise between the reduction in size and the agglomeration of nanoparticles at higher temperatures [36]. Meanwhile, the films with different thicknesses were prepared (**Fig. S5b**). Generally, the photocatalytic activity was related to the space charge layer, and when the thickness of the films was equal to the width of the space charge layer, the

photoanode exhibited the best photocatalytic activity [37]. As a result, the amount of the precursor solutions was controlled to 400  $\mu\text{L}$  in the experiments. Under the premise of ensuring the optimum film thickness and deposition temperature, the  $\text{BiVO}_4/\text{FeVO}_4$  heterojunction films with different film thickness ratios (3:1, 2:1, 1:1, 1:2, 3:1) were prepared, **Fig. 5a** displayed the photocurrent-potential (I–V) curves of  $\text{BiVO}_4/\text{FeVO}_4$  heterojunction films with varying  $\text{BiVO}_4$  layer thicknesses. With the increasing of the thickness of  $\text{BiVO}_4$  layer, the photocurrent increased obviously. However, the photocurrent density had a dramatic decrease when further increased. This performance reflected a compromise between increased absorption and increased transport limitations of thicker films. When the film thickness ratio was 1:1, the photocurrent density reached the highest value. **Fig. 5b** and **5c** showed the photocurrent-potential (I–V) curves of bare  $\text{BiVO}_4$ ,  $\text{FeVO}_4$  and  $\text{BiVO}_4/\text{FeVO}_4$  heterojunction films. The photocurrent of  $\text{BiVO}_4/\text{FeVO}_4$  heterojunction films improved to  $0.4 \text{ mA cm}^{-2}$  (at 1.23 V vs. RHE), which was more than 6 times higher than bare  $\text{BiVO}_4$  ( $0.06 \text{ mA cm}^{-2}$ ). IPCE was measured to identify the light conversion efficiency of  $\text{BiVO}_4/\text{FeVO}_4$  heterojunction electrodes, and compared to  $\text{BiVO}_4$  and  $\text{FeVO}_4$  (**Fig. 5d**). Clearly, the IPCE of the  $\text{BiVO}_4/\text{FeVO}_4$  heterojunction electrodes was much higher than that of the bare  $\text{BiVO}_4$  electrodes, confirming enhanced photoactivity. The IPCE of  $\text{BiVO}_4$  electrodes was nearly 2.5% at 450 nm. However, the IPCE of  $\text{BiVO}_4/\text{FeVO}_4$  heterojunction electrodes further increased to 13% at 450 nm. This might be attributed to the electron transfer from  $\text{FeVO}_4$  to  $\text{BiVO}_4$ , which suppressed the rapid recombination of carriers.

To quantitatively evaluate the efficiency of PEC hydrogen generation, the applied bias photon-to-current efficiency (ABPE) was calculated, as shown in **Fig. 6a**. The  $\text{BiVO}_4/\text{FeVO}_4$  heterojunction photoanode achieved the highest ABPE of 0.03% at a bias of 0.6 V versus RHE, which was equivalent to a 6-fold increase in the  $\text{BiVO}_4$  electrode.

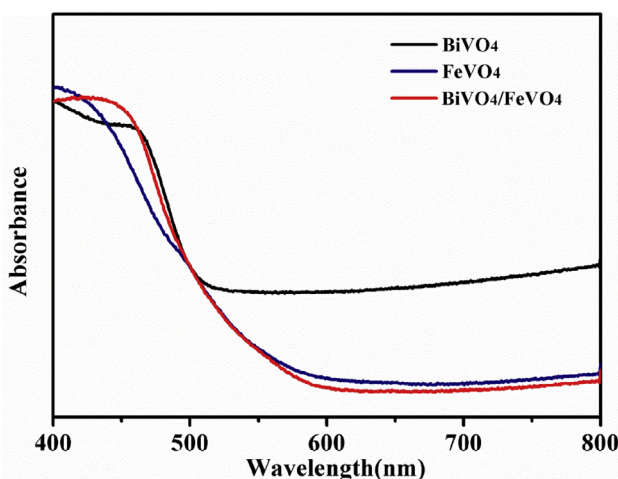


**Fig. 4 – UV–Vis spectra of bare  $\text{BiVO}_4$ ,  $\text{FeVO}_4$ , and  $\text{BiVO}_4/\text{FeVO}_4$  heterojunction films.**

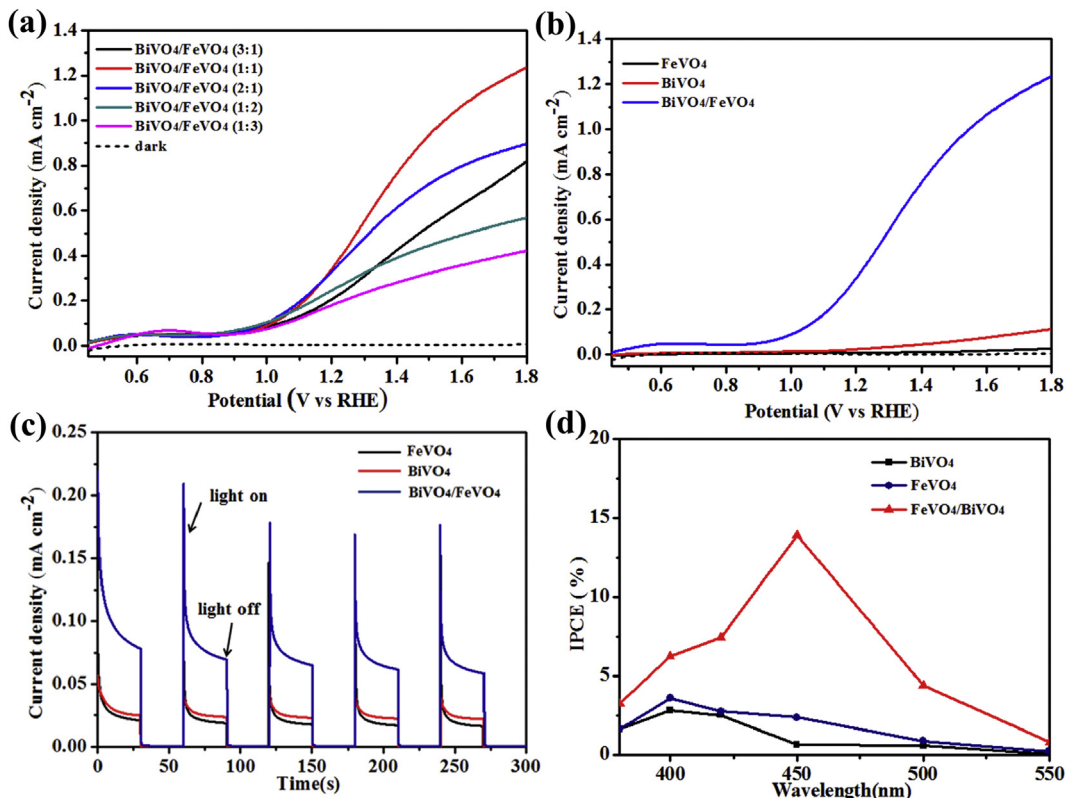


**Fig. 5 – (a)** I–V curves of BiVO<sub>4</sub>/FeVO<sub>4</sub> heterojunction films with different thickness ratios. **(b)** I–V curves, **(c)** I–T curves (at 0.8 V vs. RHE), **(d)** IPCE of bare BiVO<sub>4</sub>, FeVO<sub>4</sub> and BiVO<sub>4</sub>/FeVO<sub>4</sub> heterojunction films.

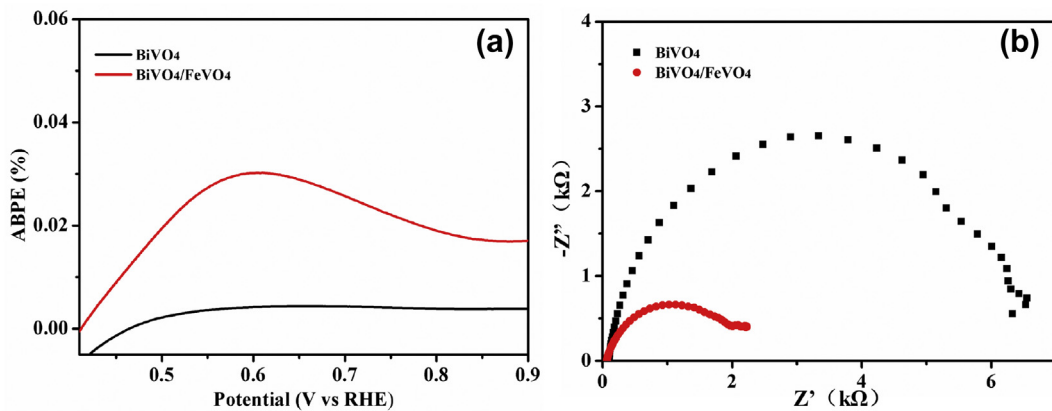


**Fig. 6 – (a)** ABPE of **(b)** Electrochemical impedance spectra of BiVO<sub>4</sub> and BiVO<sub>4</sub>/FeVO<sub>4</sub> heterojunction electrodes.

To further investigate the charge transfer and separation at the electrode-solution interface, EIS curves of bare BiVO<sub>4</sub> and BiVO<sub>4</sub>/FeVO<sub>4</sub> heterojunction electrode were measured from 0.1 to 100000 Hz under simulated solar light illumination, and the results were shown in Fig. 6b. The arc radius of bare BiVO<sub>4</sub> electrode was obviously larger than that of BiVO<sub>4</sub>/FeVO<sub>4</sub> heterojunction electrode. This indicated that the interface charge transfer and separation of the bare BiVO<sub>4</sub> electrode was significantly improved by forming a heterojunction with FeVO<sub>4</sub>.

In order to further clarify the enhancement mechanism of the PEC water splitting activity of the composite electrode, the potential energy diagram was constructed (Fig. 7.). When the composite electrode was illuminated with simulated solar light, the photogenerated electrons excited to the CB of FeVO<sub>4</sub> were injected into the CB of BiVO<sub>4</sub>, whereas holes generated on the VB of BiVO<sub>4</sub> would transfer to that of FeVO<sub>4</sub>. Therefore, the electron-hole pairs of the BiVO<sub>4</sub>/FeVO<sub>4</sub> heterojunction electrode were effectively separated, which naturally led to an increase in photoactivity.

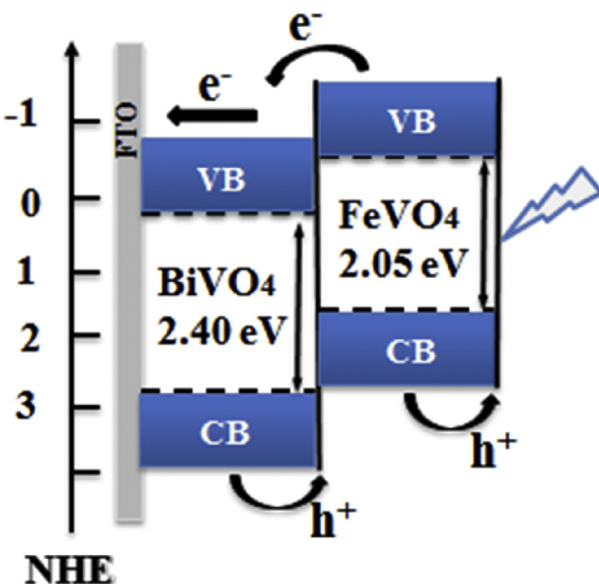


**Fig. 7 – Schematics of the potential energy diagram for the  $\text{BiVO}_4/\text{FeVO}_4$  heterojunction composite electrode.**

## Conclusions

In summary, a planar  $\text{BiVO}_4/\text{FeVO}_4$  heterostructure photoanode was prepared by electrospray technique for PEC water splitting. When the film thickness ratio was 1:1, the composite electrodes exhibited the best optical activity. The obtained maximum photocurrent density of  $0.4 \text{ mA cm}^{-2}$  at  $1.23 \text{ V}_{\text{RHE}}$  was 6 times higher than that of pristine  $\text{BiVO}_4$ , and the IPCE increased from 2.5% to 13% at 450 nm. The remarkable enhancement of PEC performance was attributed to the improvement of interface charge transfer and separation efficiency. This work provides a facile way to prepare semiconductor composites and promising route for the synthesis of spinel and perovskite materials for other applications such as Li-ion batteries, gas sensing, photochemical water purification and supercapacitors.

## Acknowledgements

This work was supported by National Natural Science Foundation of China (grants 21427802, 21671076 and 21621001).

## Appendix A. Supplementary data

Supplementary data to this article can be found online at <https://doi.org/10.1016/j.ijhydene.2019.07.063>.

## REFERENCES

- [1] Montoya JH, Seitz LC, Chakhranont P, Vojvodic A, Jaramillo TF, Norskov JK. Materials for solar fuels and chemicals. *Nat Mater* 2017;16:70–81.
- [2] Qureshy AM, Ahmed M, Dincer I. Simulation of transport phenomena in a photoelectrochemical reactor for solar hydrogen production. *Int J Hydrogen Energy* 2016;41:8020–31.
- [3] Liu LM, Wang WZ, Long JY, Fu SY, Liang YJ, Fu JL. Three-dimensional plasmonic photoanode of Au nanoparticles/ $\text{ZnFe}_2\text{O}_4$  nanosheets coated onto ZnO nanotube arrays for photoelectrochemical production of hydrogen. *Sol Energy Mater Sol Cells* 2019;195:330–8.
- [4] Li X, Yu J, Low J, Fang Y, Xiao J, Chen X. Engineering heterogeneous semiconductors for solar water splitting. *J Mater Chem* 2015;3:2485–534.
- [5] Abed J, AlMheiri M, Alexander F, Rajput NS, Viegas J, Jouiad M. Enhanced solar absorption of gold plasmon assisted  $\text{TiO}_2$ -based water splitting composite, vol. 180; 2018. p. 228–35.
- [6] Alexander F, AlMheiri M, Dahal P, Abed J, Rajput NS, Aubry C, Viegas J, Jouiad M. Water splitting  $\text{TiO}_2$  composite material based on black silicon as an efficient photocatalyst 2018;180:236–42.
- [7] Wang H, Chen F, Li W, Tian T. Gold nanocluster-sensitized  $\text{TiO}_2$  nanotubes to enhance the photocatalytic hydrogen generation under visible light. *J Power Sources* 2015;287:150–7.
- [8] Low J, Yu J, Jaroniec M, Wageh S, Al-Ghamdi AA. Heterojunction photocatalysts. *Adv Mater* 2017;1601694.
- [9] Monfort O, Pop L, Sfaelou S, Plecenik T, Roch T, Dracopoulos V, et al. Photoelectrocatalytic hydrogen production by water splitting using  $\text{BiVO}_4$  photoanodes. *Chem Eng J* 2016;286:91–7.
- [10] Lu Y, Shang H, Shi F, Chao C, Zhang X, Zhang B. Preparation and efficient visible light-induced photocatalytic activity of m- $\text{BiVO}_4$  with different morphologies. *J Phys Chem Solids* 2015;85:44–50.
- [11] Resasco J, Zhang H, Kornienko N, Becknell N, Lee H, Guo JH, et al.  $\text{TiO}_2/\text{BiVO}_4$  nanowire heterostructure photoanodes based on type II band alignment. *ACS Cent Sci* 2016;2:80–8.
- [12] He HC, Berglund SP, Rettie AJE, Chemelewski WD, Xiao P, Zhang YH, Mullins CB. Synthesis of  $\text{BiVO}_4$  nanoflake array films for photoelectrochemical water oxidation. *J Mater Chem* 2014;2:9371–9.
- [13] Park HS, Kweon KE, Ye H, Paek E, Hwang GS, Bard AJ. Factors in the metal doping of  $\text{BiVO}_4$  for improved photoelectrocatalytic activity as studied by scanning electrochemical microscopy and first-principles density-functional calculation. *J Phys Chem C* 2011;115:17870–9.
- [14] Zhong XH, He HC, Yang MJ, Ke GL, et al.  $\text{In}^{3+}$ -doped  $\text{BiVO}_4$  photoanodes with passivated surface states for photoelectrochemical water oxidation. *J Mater Chem* 2014;2:10456–65.
- [15] Huang Y, Yu YF, Xin YN, Meng NN, Yu Y, Zhang B. Promoting charge carrier utilization by integrating layered double hydroxide nanosheet arrays with porous  $\text{BiVO}_4$  photoanode for efficient photoelectrochemical water splitting. *Sci China Mater* 2017;60:193–207.
- [16] Bai SL, Liu JC, Cui M, Luo RX, He J, Chen AF. Two-step electrodeposition to fabricate the p-n heterojunction of a  $\text{Cu}_2\text{O}/\text{BiVO}_4$  photoanode for the enhancement of photoelectrochemical water splitting. *Dalton T* 2018;47:6763–71.
- [17] Pilli SK, Deutsch TG, Furtak TE, Brown LD, Turner JA, Herring AM.  $\text{BiVO}_4/\text{CuWO}_4$  heterojunction photoanodes for efficient solar driven water oxidation. *Phys Chem Chem Phys* 2013;15:3273–8.
- [18] Arunachalam M, Yun G, Ahn KS, Kang SH. Revealing the beneficial effects of  $\text{FeVO}_4$  nanoshell layer on the  $\text{BiVO}_4$  inverse opal core layer for photoelectrochemical water oxidation. *J Phys Chem C* 2017;121:7625–34.

- [19] Biswas SK, Baeg JO. Enhanced photoactivity of visible light responsive W incorporated  $\text{FeVO}_4$  photoanode for solar water splitting. *Int J Hydrogen Energy* 2013;38:14451–7.
- [20] Morton CD, Slipper IJ, Thomas MJK, Alexander BD. Synthesis and characterisation of Fe-V-O thin film photoanodes. *Photochem Photobiol* 2010;216:209–14.
- [21] Muhammad MS, Sadaf BK, Naveed AS, Nasir A, Zhang ZJ. Visible light assisted photocatalytic degradation of crystal violet dye and electrochemical detection of ascorbic acid using a  $\text{BiVO}_4/\text{FeVO}_4$  heterojunction composite. *RSC Adv* 2018;8:23489–98.
- [22] Santato C, Odziedkowski M, Ullmann M, Augustynski J. Crystallographically oriented Mesoporous  $\text{WO}_3$  films: synthesis, characterization, and applications. *J Am Chem Soc* 2001;123:10639–49.
- [23] Xiong LB, Li SM, Li BH, Zeng QD, Wang BY, Nie CJ. Preparation by a simplified hydro-thermal method and photoelectrochemical properties of n-type  $\text{Cu}_2\text{O}$  film. *Chin J Inorg Chem* 2018;34:1271–8.
- [24] Cao JY, Kako T, Li P, Ouyang SX, Ye JH. Fabrication of p-type  $\text{CaFe}_2\text{O}_4$  nanofilms for photoelectrochemical hydrogen generation. *Electrochim Commun* 2011;13:275–8.
- [25] Peeters D, Taffa DH, Kerrigan MM, Ney A, et al. Photoactive zinc ferrites fabricated via conventional CVD approach. *ACS Sustain Chem Eng* 2017;5:2917–26.
- [26] Sang LX, Zhang HJ, Ni XC, Anoop KK, Rosalba F, Wang X, Salvatore A. Hydrogen-evolving photoanode of  $\text{TiO}_2$  nanoparticles film deposited by a femtosecond laser. *Int J Hydrogen Energy* 2015;40:779–85.
- [27] Jennifer L, Yakup G, Pedram G, Sanjay M. Electronically-coupled phase boundaries in alpha- $\text{Fe}_2\text{O}_3/\text{Fe}_3\text{O}_4$  nanocomposite photoanodes for enhanced water oxidation. *ACS Appl Nano Mater* 2019;21:334–42.
- [28] Zheng FQ, Wang D, Fang HR, Wang HD, Wang M, Huang KK, Chen HW, Feng SH. Controlled crystallization of sodium chloride nanocrystals in microdroplets produced by electrospray from an ultra-dilute solution. *Inorg Chem* 2016;12:1860–5.
- [29] Fang HR, Huang KK, Yuan L, Wu XF, Wang D, Chen HW, Feng SH. The direct synthesis of Au nanocrystals in microdroplets using the spray-assisted method. *New J Chem* 2016;40:7294–8.
- [30] Wang M, Wu XF, Huang KK, Sun Y, Zhang Y, Zhang H, He JJ, Chen HW, Ding JH, Feng SH. Enhanced solar water-splitting activity of novel nanostructured  $\text{Fe}_2\text{TiO}_5$  photoanode by electrospray and surface F-modification. *Nanoscale* 2018;10:6678–83.
- [31] Fan HM, Jiang TF, Li HY, Wang DJ, Wang LL, Zhai JL, et al. Effect of  $\text{BiVO}_4$  crystalline phases on the photoinduced carriers behavior and photocatalytic activity. *J Phys Chem C* 2012;116:2425–30.
- [32] Santato C, Ullmann M, Augustynski J. Photoelectrochemical properties of nanostructured tungsten trioxide films. *J Phys Chem B* 2001;105:936–40.
- [33] Chen L, Meng D, Wu X, Wang A, Wang J, Wang Y, Yu M. In situ synthesis of  $\text{V}^{4+}$  and  $\text{Ce}^{3+}$  self-doped  $\text{BiVO}_4/\text{CeO}_2$  heterostructured nano composites with high surface areas and enhanced visible-light photocatalytic activity. *J Phys Chem C* 2016;120:18548–59.
- [34] Mishra M, Park H, Chun DM. Photocatalytic properties of Au/ $\text{Fe}_2\text{O}_3$  nano-composites prepared by Co-precipitation. *Adv Powder Technol* 2016;27:130–8.
- [35] Shan L, Liu H, Wang G. Preparation of tungsten-doped  $\text{BiVO}_4$  and enhanced photocatalytic activity. *J Nanopart Res* 2015;17:181.
- [36] Zhang P, Gao L, Song XF, Sun J. Micro-and nanostructures of photoelectrodes for solar-driven water splitting. *Adv Mater* 2015;27:562–8.
- [37] Saremi Yarahmadi S, Wijayantha KGU, Tahir AA, Vaidhyanathan B. Nanostructured alpha- $\text{Fe}_2\text{O}_3$  electrodes for solar driven water splitting: effect of doping agents on preparation and performance. *J Phys Chem C* 2009;113:4768–78.